Structural determinants of ligand binding selectivity between the peroxisome proliferator-activated receptors

H. Eric Xu*, Millard H. Lambert†, Valerie G. Montana, Kelli D. Plunket, Linda B. Moore, Jon L. Collins, Jeffery A. Oplinger, Steven A. Kliewer, Robert T. Gampe, Jr., David D. McKee, John T. Moore, and Timothy M. Willson‡

Nuclear Receptor Discovery Research, GlaxoSmithKline, Research Triangle Park, NC 27709

Edited by Michael G. Rosenfeld, University of California at San Diego, La Jolla, CA, and approved September 27, 2001 (received for review August 3, 2001)

The peroxisome proliferator-activated receptors (PPARs) are transcriptional regulators of glucose, lipid, and cholesterol metabolism. We report the x-ray crystal structure of the ligand binding domain of PPARα (NR1C1) as a complex with the agonist ligand GW409544 and a coactivator motif from the steroid receptor coactivator 1. Through comparison of the crystal structures of the ligand binding domains of the three human PPARs, we have identified molecular determinants of subtype selectivity. A single amino acid, which is tyrosine in PPARα and histidine in PPARγ, imparts subtype selectivity for both thiazolidinedione and nonthiazolidinedione ligands. The availability of high-resolution cocrystal structures of the three PPAR subtypes will aid the design of drugs for the treatments of metabolic and cardiovascular diseases.

Peroxisome proliferator-activated receptor (PPAR) α (NR1C1), PPARγ (NR1C3), and PPARδ (NR1C2) are members of the nuclear receptor family of ligand-activated transcription factors that bind to fatty acids (FAs) and their metabolites (1). Although the PPARs were originally cloned as orphan receptors, their role in mammalian physiology has been uncovered through a process of reverse endocrinology (2) using high-affinity synthetic ligands as chemical tools. PPARα is the receptor for the fibrate class of lipid-lowering drugs (3), and PPARγ is the receptor for the thiazolidinedione (TZD) class of antidiabetic drugs (4). Recently, the function of PPARδ in the regulation of reverse cholesterol transport and high-density lipoprotein metabolism was revealed through the use of a potent PPARδ agonist, GW501516 (5). Thus, the PPARs are FA-activated receptors that function as key regulators of glucose, lipid, and cholesterol metabolism.

The marketed TZDs rosiglitazone and pioglitazone are effective glucose-lowering drugs that produce modest effects on lipids in patients with type 2 diabetes (1). Most diabetic patients have an abnormal lipid profile, including low levels of high density lipoprotein and high levels of triglycerides, which may contribute to their greatly increased burden of cardiovascular disease. There is a resurgence of interest in the development of new antidiabetic drugs that combine the insulin-sensitizing effects of PPARγ activation with the additional lipid-modifying activity of the other PPAR subtypes. For example, the L-tyrosine analogue farglitazar (GI262570) has robust effects on glucose, high-density lipoprotein, and triglycerides in diabetic patients (6). The triglyceride-lowering activity of farglitazar may be a result of its activity on PPARα. Although farglitazar is 1,000 times less potent on PPARα, its peak plasma levels are above the EC_{50} for activation of this subtype (1, 6). Additional insight into the molecular determinants of PPAR subtype selectivity may have important applications in the design of new diabetes drugs.

X-ray crystal structures of the PPARγ and PPARδ ligand binding domains (LBDs) revealed that the receptors contain a much larger ligand binding pocket than other nuclear receptors (7–10). The size of this pocket may explain the ability of the PPARs to bind a variety of naturally occurring and synthetic lipophilic acids. Remarkably, PPARα has been reported to bind to an even wider range of FAs than either PPARγ or PPARδ (10). However, no structure of the PPARα LBD has been available to explain these differences in ligand binding properties. We now report the structure of the PPARα LBD and the identification of key determinants of ligand binding selectivity between the three PPAR subtypes.

Materials and Methods

Reagents and Assays. Rosiglitazone, pioglitazone, and farglitazar were synthesized as described (11). The synthesis of GW409544 will be described elsewhere. Expression plasmids for the human PPAR-GAL4 chimeras were prepared by inserting amplified cDNAs encoding the LBDs into a modified pSG5 expression vector (Stratagene) containing the GAL4 DNA binding domain (amino acids 1–147) and the simian virus 40 large T antigen nuclear localization signal (APKKKRKVG). For generation of the Y314H PPARα mutant, the Tyr-314 codon (TAT nucleotide sequence) was altered to a His codon (CAT) by Quick-Change Mutagenesis (Stratagene). For generation of the H323Y PPARγ mutant the His-323 codon (CAC) was altered to a Tyr codon (TAC). Cell-based reporter assays were performed by transient transfection in CV-1 cells using $(UAS)_5$-tk-SPAP reporter constructs as described (11). Transfections were performed using Lipofectamine (Life Technologies, Grand Island, NY) according to the manufacturer's instructions. A β-galactosidase expression plasmid was included in each transfection for use as a normalization control.

Protein Expression. The human PPARα LBD (amino acids 192–468 of GenBank No. S74349) tagged with MKKGHHHHHHG was expressed from the T7 promoter of plasmid vector pRSETA. Bacterial cells (BL21DE3) transformed with this expression vector were grown at 24°C in 2YT broth with 50 mg/liter carbenicillin in shaker flasks to an OD_{600} of ≈5.0. Cells were harvested, resuspended with 20 ml of extract buffer (20 mM Hepes, pH 7.5/50 mM imidazole/250 mM NaCl, and a trace of lysozyme) per liter of cells and sonicated for 20 min on ice. The lysed cells were centrifuged at 40,000 × *g* for 40 min, and the supernatant was loaded on a 100-ml Ni-agarose column. The

This paper was submitted directly (Track II) to the PNAS office.

Abbreviations: PPAR, peroxisome proliferator-activated receptor; TZD, thiazolidinedione; LBD, ligand binding domain; FA, fatty acid; SRC1, steroid receptor coactivator 1.

Data deposition: The atomic coordinates and structure factors have been deposited in the Protein Data Bank, www.rcsb.org (PDB ID codes 1K7L and 1K74).

*To whom correspondence on the structure determination and requests for materials should be addressed. E-mail: ex11957@gsk.com.

†To whom correspondence on molecular modeling should be addresssed. E-mail: mhl8097@gsk.com.

‡To whom additional correspondence and reprint requests should be addressed. E-mail: tmw20653@gsk.com.

The publication costs of this article were defrayed in part by page charge payment. This article must therefore be hereby marked "*advertisement*" in accordance with 18 U.S.C. §1734 solely to indicate this fact.

column was washed with 150 ml of buffer A (10% glycerol/20 mM Hepes, pH 7.5/25 mM imidazole), and the protein was eluted with a 450-ml gradient to buffer B (10% glycerol/20 mM Hepes, pH 7.5/500 mM imidazole). The protein, which eluted at 20% buffer B, was diluted with 1 vol of buffer C (20 mM Hepes, pH 7.5/1 mM EDTA) and loaded on a 100-ml S-Sepharose column. The column was washed with a 100-ml buffer C, and the PPARα LBD was eluted with a 200-ml gradient to buffer D (20 mM Hepes, pH 7.5/10 mM DTT/1 M ammonium acetate). The PPARα LBD was eluted from the column at 43% buffer D, which yielded 9 mg of protein per liter of cells, and was >95% pure as determined by SDS/PAGE analysis. The protein was then diluted to 1 mg/ml with buffer C such that the final buffer composition was 220 mM ammonium acetate/20 mM Hepes, pH 7.5/1 mM EDTA/1 mM DTT. The diluted protein was aliquoted, frozen, and stored at −80°C. The protein–ligand complexes were prepared by adding 5-fold excess of GW409544 and a 2-fold excess of a peptide from the steroid receptor coactivator 1 (SRC1) containing the sequence HSSLTERHKILHRLLQEGSPS (LxxLL motif underlined) and were concentrated to 10 mg/ml. The PPARγ/RXRα heterodimer complex with GW409544 and 9-*cis*-retinoic acid was prepared as reported (9).

Crystallization and Data Collection. The PPARα/GW409544/SRC1 crystals were grown at room temperature in hanging drops containing 1 μl of the protein–ligand solution and 1 μl of well buffer (50 mM bis-Tris-propane, pH 7.5/4–6% PEG 3350/150 mM $NaNO_3$/16% 2,5-hexanediol/1–3 mM YCl_3). Before data collection, crystals were transiently mixed with the well buffer that contained an additional 10% hexanediol and then were flash-frozen in liquid nitrogen.

The PPARα crystals formed in the $P2_12_12_1$ space group, with a = 95.58 Å, b = 122.06Å, and c = 122.10 Å. Each asymmetry unit contains four molecules of the PPARα LBD with 50% of solvent content. The PPARγ/RXRα heterodimer crystals, which were prepared as reported (9), formed in the $P2_12_12_1$ space group with a = 46.62 Å, b = 55.10 Å, and c = 214.86 Å. Data were collected with a MAR charge-coupled device detector at 17-ID in the facilities of the Industrial Macromolecular Crystallography Association Collaborative Access Team at the Advanced Photon Source (Argonne National Laboratory, Argonne, IL). The observed reflections were reduced, merged, and scaled with DENZO and SCALEPACK in the HKL2000 package (12).

Structure Determination and Refinement. The structure of the PPARα/GW409544/SRC1 complex was determined by molecular replacement methods with the CCP4 AMORE program (13) using the PPARδ LBD structure as the initial model (10). Model building was carried out with QUANTA (Molecular Simulations, Waltham, MA), and refinement was progressed with CNX (14) and multiple cycles of manual rebuilding. The structure of the PPARγ/RXRα heterodimer complex with GW409544 and 9-*cis*-retinoic acid was determined by using the PPARγ/RXRα/farglitazar/SRC1 structure in the molecular replacement search (9). The statistics of both structures are summarized in Table 1.

Computational Analysis. The ligand binding pocket was defined with the MVP program (15), and the resulting surface and volume were calculated with the Connolly MS program (16) and GRASP (17), respectively.

Results

Structures of GW409544 Bound to PPARα and PPARγ. The L-tyrosine analogue farglitazar (1) is a full agonist of PPARγ and PPARα, although it is much less potent on the latter receptor (Fig. 1*A* and Table 2). Modification of the farglitazar structure led to the L-tyrosine analogue GW409544 (Fig. 1*B*), which is a potent full agonist on both PPARα and PPARγ (J.A.O. and J.L.C., unpublished results). GW409544 contains a vinylogous amide as the L-tyrosine *N*-substituent, which contains three fewer carbon atoms than the benzophenone found in farglitazar. Aside from this difference, the chemical structures of the compounds are identical. GW409544 activates PPARα with EC_{50} = 2.3 nM and PPARγ with EC_{50} = 0.28 nM, but shows no activation of PPARδ at concentrations up to 10 μM (Fig. 1*B* and Table 2). To understand the structural basis of the PPAR subtype selectivity of GW409544, we determined its cocrystal structure with the LBDs of both PPARα and PPARγ.

Table 1. Statistics of crystallographic data and structures

Crystals	PPARα/SRC1 with GW409544	PPARγ/RXRα/SRC1 with GW409544
Space group	$P2_12_12_1$	$P2_12_12_1$
Resolution, Å	20.0–2.5	20.0–2.3
Unique reflections, *N*	49,991	24,986
Completeness, %	99.9	97.3
I/σ (last shell)	48.3 (5.7)	28.9 (3.3)
R_{sym}*, %	5.4	5.7
Refinement statistics		
R factor†, %	24.7	23.8
R free, %	28.5	27.9
rmsd‡ bond lengths, Å	0.012	0.011
rmsd bond angles, °	1.550	1.515
Total nonhydrogen atoms	9312	4408

*$R_{sym} = \Sigma|Iavg - Ii|/\Sigma Ii$.

†$R_{factor} = \Sigma|F_P - F_{Pcalc}|/\Sigma F_p$, where F_p and F_{pcalc} are observed and calculated structure factors, R_{free} is calculated from a randomly chosen 10% of reflections excluded from the refinement, and R_{factor} is calculated for the remaining 90% of reflections.

‡rmsd, the rms deviation from ideal geometry.

A 2.5-Å crystal structure of the PPARα LBD was solved as a ternary complex with GW409544 and an LxxLL peptide derived from SRC1 (18). The PPARα protein is composed of a helical sandwich and a four-stranded β-sheet, as was seen in the PPARγ (7–9) and PPARδ (10) crystal structures (Fig. 2*A*). Within the LBD is a large pocket of ≈1,400 Å^3 into which the small molecule ligand is bound. Clear electron density was observed for GW409544 (Fig. 2*B*). The ligand adopts a conformation within the receptor that allows the acidic head group to form hydrogen bonds with Tyr-314 on helix 5 and Tyr-464 on the AF2 helix (Fig. 2 *A* and *C*). These interactions stabilize the AF2 helix in a conformation that generates a charge clamp between Glu-462 and Lys-292, which in turn directs the binding of the LxxLL peptide to a hydrophobic cleft on the surface of the receptor. Thus, the hydrogen bonds between the carboxylate of GW409544 and the PPARα protein act as a molecular switch to activate the transcriptional activity of the receptor. The vinylogous amide on the tyrosine nitrogen of GW409544 reaches into a hydrophobic pocket formed by helices 3, 6, and 10 adjacent to the C-terminal AF2 helix. This pocket corresponds to the "benzophenone" pocket in the PPARγ/farglitazar structure (9). The remainder of the ligand wraps around helix 3 and buries the phenyloxazole tail into a lipophilic pocket formed by helices 2′, 3, and the β sheet (Fig. 2 *A* and *C*).

A 2.3-Å crystal structure of the PPARγ LBD/RXRα LBD heterodimer was solved as a complex with GW409544, 9-*cis*-retinoic acid and two LxxLL peptides from SRC1 (Fig. 3*A*). The overall structure is similar to the PPARγ/RXRα heterodimer complex bound to farglitazar and 9-*cis*-retinoic acid (9), with both complexes showing the same architecture and heterodimer interface. As in the PPARα structure, clear electron density was observed for GW409544 within PPARγ (Fig. 3*B*). The ligand adopts a similar orientation, with hydrogen bonds between the acidic head group and His-323 on helix 5 and Tyr-473 on the AF2

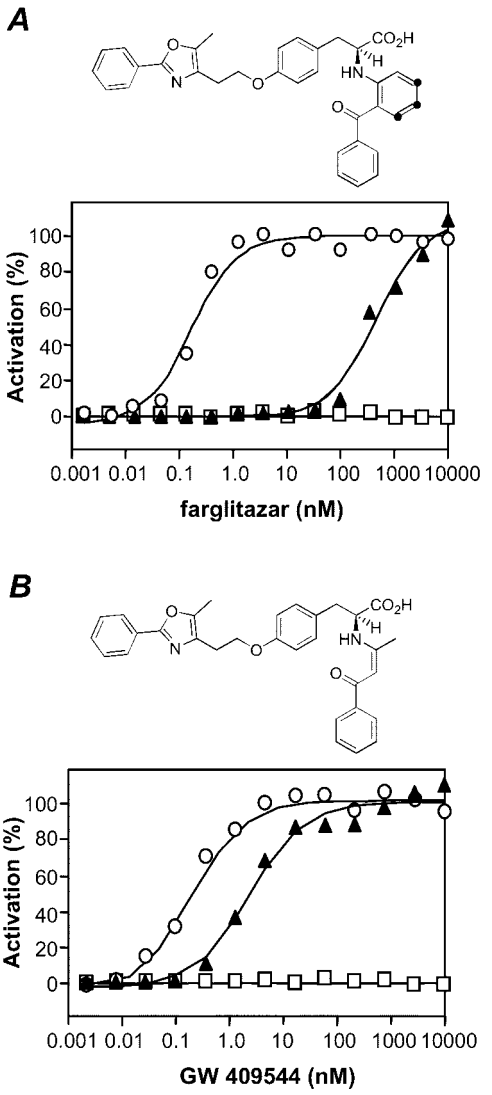

Fig. 1. Activation of human PPAR-GAL4 chimeric receptors by L-tyrosine PPAR agonists: PPARα (▲), PPARγ (○), and PPARδ (□); 100% response corresponds to 6-, 7-, and 12-fold activation of the reporter gene by PPARα, PPARγ, and PPARδ, respectively. (*A*) Chemical structure and PPAR activation profile for farglitazar. The three carbon atoms removed to increase PPARα activity are marked by black dots. (*B*) Chemical structure and PPAR activation profile for GW409544.

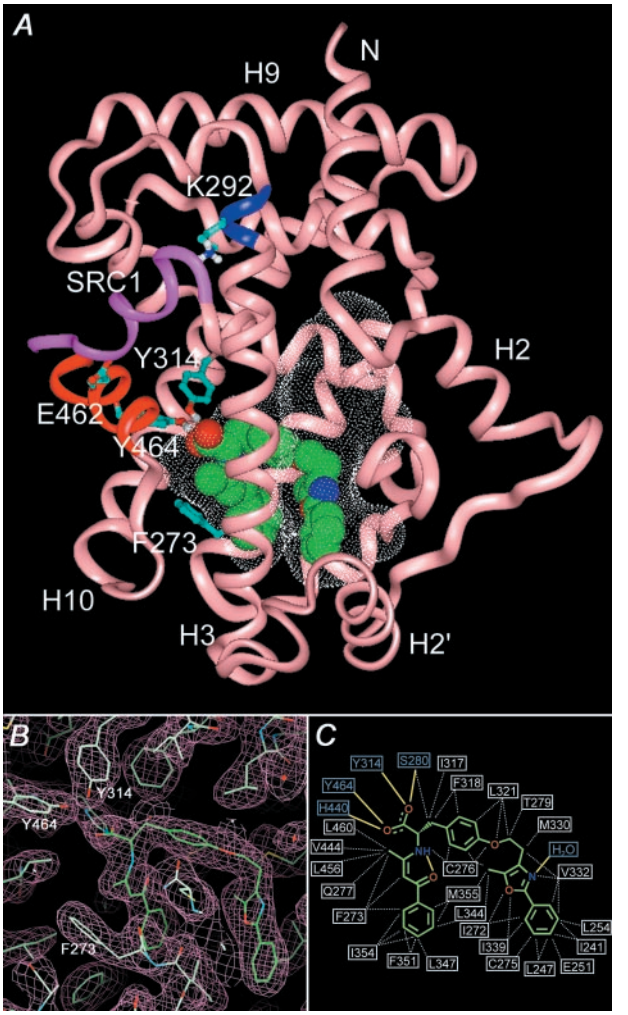

Fig. 2. X-ray crystal structure of the PPARα LBD. (*A*) The PPARα protein is displayed as a red worm with the AF2 helix in red and K292 in dark blue. The LxxLL peptide is displayed as a purple worm. The agonist ligand GW409544 is displayed in space-filling representation colored by atom type. The solvent-accessible ligand binding pocket is shown as a white dot surface. Helices 2, 2′, 3, 9, and 10 are indicated. The amino acids Phe-273, Lys-292, Tyr-314, Glu-462, and Tyr-464 are displayed in light blue. (*B*) A $2F_o - F_c$ omit map showing the electron density (1σ) of the ligand and the surrounding residues. (*C*) Key hydrogen bonding (yellow line) and hydrophobic (white broken line) interactions between GW409544 and the PPARα protein and a bound water molecule.

helix serving to stabilize the C-terminal helix in an active conformation (Fig. 3*A* and *C*). The vinylogous amide substituent in GW409544 occupies, but does not completely fill, the benzophenone pocket formed by helices 3, 7, and 10 (Fig. 3*A*). The remaining interactions with PPARγ and the conformation of GW409544 are almost identical to those observed for farglitazar within the PPARγ/RXRα heterodimer (Fig. 3*C*). The conformation of the phenyloxazole side chain is identical for GW409544 in the PPARα and PPARγ/RXRα structures.

Table 2. Activity of L-tyrosine and TZD ligands on human PPARs

Receptor	Farglitazar EC_{50}, nM	GW409544 EC_{50}, nM	Rosiglitazone EC_{50}, nM	Pioglitazone EC_{50}, nM
PPARα	250 ± 35	2.3 ± 0.5	>10,000	>10,000
PPARα Y314H	3.8 ± 0.8	2.1 ± 0.5	1200 ± 300	3,000 ± 300
PPARγ	0.20 ± 0.05	0.28 ± 0.06	18 ± 4	280 ± 42
PPARγH323Y	6.2 ± 1.5	0.55 ± 0.10	900 ± 250	2,200 ± 1,100
PPARδ	>10,000	>10,000	>10,000	>10,000

Data are represented as the EC_{50} for activation of the corresponding human PPAR-GAL4 chimeric receptor ± S.E. for $n = 3$. Compounds with $EC_{50} < 1{,}000$ nM tested as full agonists compared to standard controls.

Structural Basis for PPAR Subtype Selectivity. The three PPAR subtypes have 60–70% sequence identity between their LBDs. Although all three subtypes bind to naturally occurring FAs (10), synthetic ligands have been developed with a range of subtype selectivities (1). Comparison of the three-dimensional structures of the three PPAR LBDs (Fig. 4*A*) shows that although the overall size of the pockets is similar there are marked differences in the detailed topology. Most notably, the PPARδ pocket is narrower in the region adjacent to the AF2 helix. As a result, PPARδ is unable to accommodate the bulky nitrogen substituents that are present on the tyrosine-based ligands farglitazar

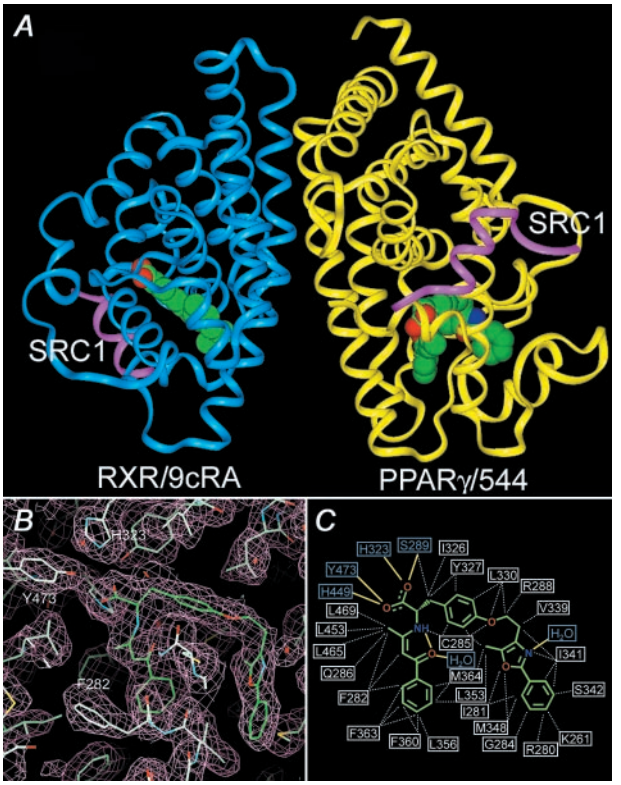

Fig. 3. X-ray crystal structure of the PPARγ/RXRα LBDs. (*A*) The PPARγ protein is displayed as a yellow worm and the RXRα protein as a dark blue worm with the LxxLL peptides in purple. The agonist ligands GW409544 and 9-*cis*-retinoic acid are displayed in space-filling representations colored by atom type. (*B*) A $2F_o - F_c$ omit map showing the electron density (1σ) of the ligand and the surrounding residues. The amino acids Phe-282, Tyr-323, and Tyr-473 are indicated. (*C*) Key hydrogen bonding (yellow line) and hydrophobic (white broken line) interactions between GW409544 and the PPARγ protein and two bound water molecules.

and GW409544, which explains why neither compound has significant binding affinity or functional activity on this subtype (Table 2 and data not shown).

Farglitazar is a potent activator of PPARγ that shows ≈1,000-fold selectivity over PPARα (Fig. 1*A* and Table 2). In contrast, GW409544 is a potent activator of both PPARα and PPARγ, with <10-fold difference between its PPARα and PPARγ activity. To explain the dramatic difference in subtype selectivity between two closely related small molecule ligands, we generated superpositions of the PPARα and PPARγ crystal structures by overlaying their protein backbones. Although there was an rms deviation of only 0.84 Å over the total protein backbones of PPARα and PPARγ (excluding the variable loop between helix 2 and helix 3), a significant difference in the positioning of farglitazar and GW409544 was observed (Fig. 4*B*). Because of the larger steric size of Tyr-314 in PPARα compared with His-323 in PPARγ, GW409544 occupies a position in which it lies 1.5 Å deeper into the PPARα ligand binding pocket than the position of farglitazar in the PPARγ pocket (Fig. 4*B*). Molecular modeling (15) indicates that farglitazar cannot shift in the PPARα pocket because of a steric clash with Phe-273, which caps the benzophenone pocket adjacent to the AF2 helix (Fig. 4*B*). Remarkably, the three carbon atoms, which were removed from farglitazar to generate GW409544, are responsible for this unfavorable steric interaction. Thus, the potent dual PPARα/γ agonist activity of GW409544 is the result of a reengineering of the ligand to accommodate the larger size of the Tyr-314 residue in PPARα (Fig. 4*C*).

Comparison of the amino acids lining the ligand binding pockets of PPARα and PPARγ (Figs. 2*C* and 3*C*) shows that there are several conservative and nonconservative changes between the subtypes. To further explore the concept that a single residue might account for the subtype selectivity observed with the L-tyrosine PPAR agonists, a single point mutation was introduced in both receptors: Y314H in PPARα and H323Y in PPARγ. When assayed on the Y314H PPARα mutant, farglitazar was a potent full agonist with a 66-fold lower EC_{50} compared with the wild-type PPARα (Table 2). The converse was seen with the H323Y PPARγ. Farglitazar was a 31-fold less potent full agonist on the H323Y mutant compared with wild-type PPARγ. Thus, the PPAR selectivity of farglitazar depends, to a large degree, on the presence of histidine rather than tyrosine at the carboxylate-binding residue in helix 5. As expected from the structural analysis of PPARα and PPARγ, the reengineered side chain of GW409544 was accommodated by both the mutant and wild-type receptors with little change in potency or efficacy.

The TZDs rosiglitazone and pioglitazone are selective PPARγ agonists with no measurable activity on PPARα (Table 2). The x-ray crystal structure of rosiglitazone complexed to PPARγ (7, 9) shows that it binds in a similar orientation to farglitazar and GW409544, in which the acidic TZD heterocycle forms hydrogen bonds with His-323 on helix 5 and Tyr-473 on the AF2 helix. However, unlike the tyrosine-based ligands, the TZD head group does not occupy the benzophenone pocket. Surprisingly, the TZDs showed micromolar activity on both Y314H PPARα and H323Y PPARγ (Table 2). Although they are ≈100-fold less potent than farglitazar, the TZDs showed shifts in activity that parallel the data obtained with the L-tyrosine agonist. These results suggest that the determinants of PPAR subtype selectivity are conserved between the TZD and non-TZD classes of ligands.

Discussion

The mammalian PPARs display pharmacologically distinct activation profiles by natural and synthetic ligands (1, 19). Solution of the x-ray crystal structure of the PPARα LBD allows a comparison of the molecular basis of this subtype selectivity across the three PPARs (Fig. 4*A*). The PPARα and PPARγ ligand binding pockets are significantly larger than the PPARδ pocket because of the narrowing of the pocket adjacent to the AF2 helix. It is notable that only a handful of potent PPARδ ligands have been described (1). Ligands such as TZDs and L-tyrosine-based agonists show little or no binding to PPARδ (Fig. 1 and Table 2). In both cases, their acidic head groups seem to be too large to fit within the narrow PPARδ pocket. In contrast, the potent PPARδ agonist GW501516 contains an unsubstituted phenoxyacetic acid head group that complements the narrow PPARδ ligand binding pocket (5). Fibrate ligands, which generally bind to PPARδ only at high micromolar concentrations (1), contain small alkyl substituents adjacent to the carboxylate group. We have previously identified the mutation M417V, which allows fibrate ligands to bind to PPARδ (20). This mutation is likely to increase the size of the PPARδ pocket to facilitate the binding of the small alkyl substituents adjacent to the carboxylate. Thus, the reduced size of the PPARδ pocket is a major determinant of ligand binding to this subtype.

The design of dual PPARα/γ agonists is of major medical interest, as these compounds may combine the benefits of the glitazone and fibrate classes of drugs within a single molecule (1). In comparison with PPARδ, the PPARα and PPARγ ligand binding pockets are closer in size and shape to each other. We have found that a major determinant of selectivity between these two subtypes is the substitution of Tyr-314 in PPARα for His-323 in PPARγ. These amino acids form part of the network of hydrogen-bonding residues that are involved in the activation of

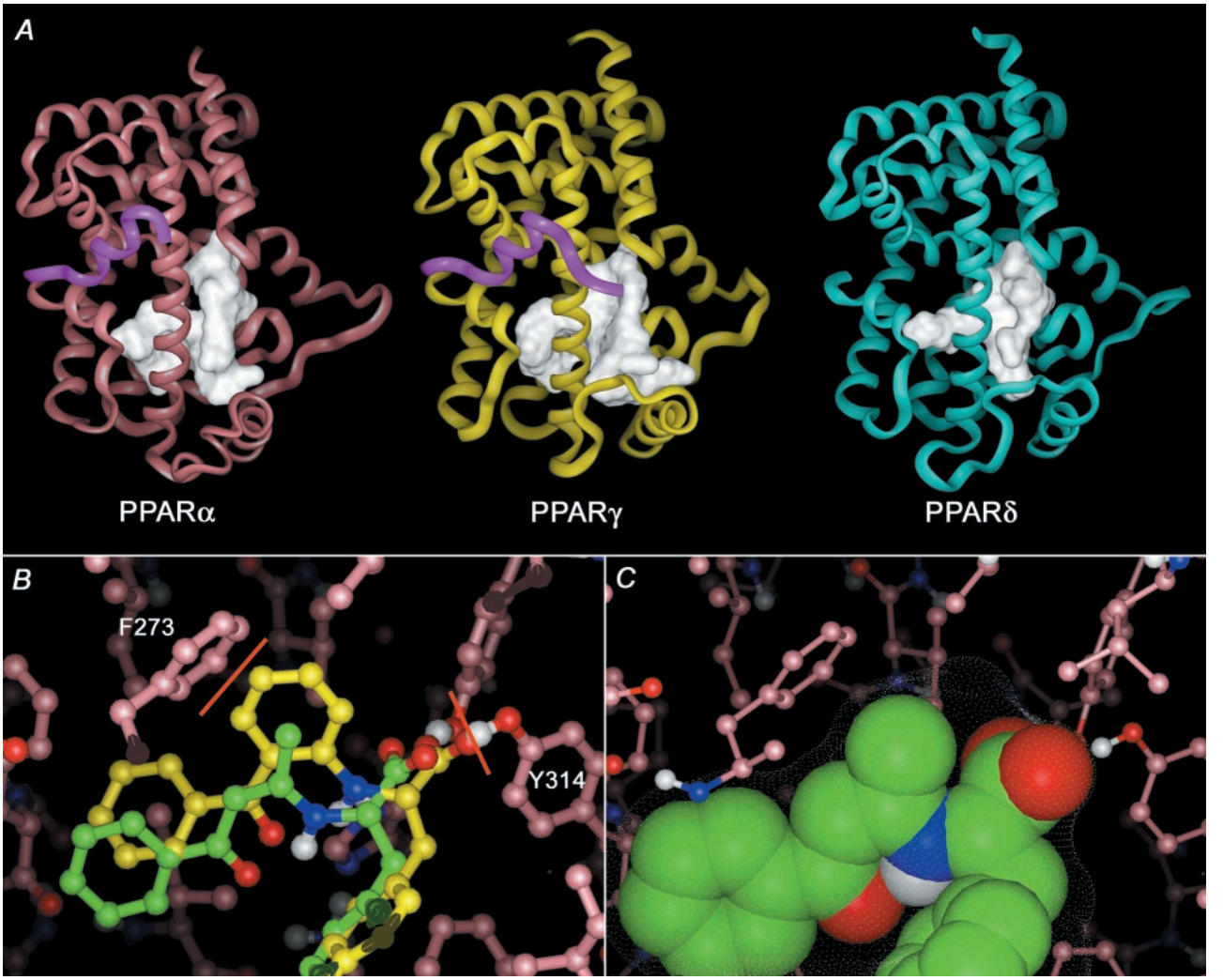

Fig. 4. Molecular determinants of PPAR subtype selectivity. (*A*) Comparison of the x-ray crystal structures of PPARα (red worm), PPARγ (yellow worm), and PPARδ (blue worm). Each PPAR is complexed to a high-affinity ligand (not shown). PPARα and PPARγ are complexed to LXXLL peptides (purple worms). For each PPAR, the solvent-accessible ligand binding pocket is displayed as an off-white surface. (*B*) Superposition of farglitazar in PPARγ with GW409544 in PPARα. Phe-273 and Tyr-314 are indicated, with the proposed steric interactions with farglitazar shown as red lines. (*C*) The x-ray crystal structure of reengineered L-tyrosine ligand GW409544 in the ligand binding pocket of PPARα. GW409544 is displayed in space-filling representation colored by atom type. The solvent-accessible ligand binding pocket is shown as a white dot surface.

the receptor by its acidic ligands. Overlay of the PPARα and PPARγ crystal structures reveals that the larger volume of the Tyr-314 side chain in PPARα forces a 1.5-Å shift in the position of the high-affinity ligand GW409544. Remarkably, it is the ligand that shifts rather than the protein backbone. The structurally related ligand farglitazar is unable to accommodate this shift because of a steric interaction with PPARα Phe-273. As a result, farglitazar shows 1,000-fold selectivity for PPARγ over PPARα. Point mutation of Y314H in PPARα and H323Y in PPARγ demonstrate that these single amino acids are, in large part, responsible for determining the subtype selectivity of farglitazar. In each case, a 1–2 log shift in the potency of the ligand was observed. Compared with farglitazar, GW409544 has three atoms removed to allow it to shift within the PPARα pocket without clashing with Phe-273. The potent dual PPARα/γ agonist activity of GW409544 results from a complementary match of the reengineered ligand with both the PPARα and PPARγ ligand binding pockets. The use of similar ligand engineering may have utility in the development of other designer receptor–ligand pairs (21).

TZD ligands do not contain the large *N*-substituents present in the L-tyrosine-based ligands (1). Remarkably, rosiglitazone and pioglitazone still respond to the point mutation of Y314H in PPARα and H323Y in PPARγ with a corresponding increase in PPARα and decrease in PPARγ activity, respectively. These data suggest that the TZDs also have difficulty accommodating the 1.5-Å shift required to bind to PPARα. We speculate that the shift in the TZD head group results in an unfavorable conformation in the remainder of the molecule. Notably, the TZD KRP-297 was recently reported to show dual PPARα/γ activity (22). Unlike rosiglitazone and pioglitazone, which are *para*-substituted across their central phenyl rings, KRP-297 has a *meta*-substituted side chain (1), which may allow an improved fit in the PPARα protein.

Although all three PPAR subtypes bind to polyunsaturated FAs with micromolar affinity, only PPARα binds to a wide range of saturated FAs (10). This property may be important for its proposed role in the regulation of hepatic lipid metabolism in response to saturated fats (10, 23–25). The PPARα pocket is more lipophilic and less solvent exposed than the corresponding

pockets of either PPARγ or PPARδ (Fig. 3*A*). For example, the solvent-exposed ligand entry channel in PPARα is partially shielded by Tyr-334. In addition, several hydrophilic residues that contact the ligand in PPARγ are converted into more hydrophobic residues in PPARα (Figs. 2*C* and 3*C*). The more hydrophobic nature of the PPARα pocket may explain why it does not bind to certain hydroxylated FAs, which are good ligands for PPARγ (25). Thus, among the three subtypes, PPARα may be best suited to bind to the more lipophilic saturated FAs. Saturated FAs also have different low energy conformations compared with their unsaturated counterparts (10), some of which may be able to accommodate changes in the PPARα ligand binding pocket imposed by the larger volume of Tyr-314. Interestingly, a putative yeast FA binding protein Pex11p (26), which has extensive amino acid sequence homology to the PPARs (27), conserves all of the carboxylate binding residues found in PPARα. One might speculate that an ancestral PPAR also contained a single histidine and two tyrosines as carboxylate binding residues. In this case, the mutation of tyrosine to histidine in PPARγ/PPARδ may have resulted from an evolutionary drive for these subtypes to bind preferentially to unsaturated FAs (10).

Finally, it is interesting to note that a single amino acid difference in PPARs has such a dramatic impact on ligand selectivity, given that the PPAR pocket is composed of more than 25 aa. Other examples where the specificity of a macromolecular interaction is determined by a single amino acid difference can be found in the protein–DNA interactions of certain transcription factors. It is well documented for homeodomains and pair domains that their DNA binding specificity is controlled by a single residue difference in the recognition helix of their helix–turn–helix motifs (28–30). In these protein–DNA interactions, the residue that determines the binding specificity forms specific hydrogen bonds with the DNA base pairs (31–33). In the PPARs, the general hydrogen bond patterns are kept constant, and the specificity of ligand binding arises from small changes in the position of the ligand when docked into the different shaped pockets. This observation may not be unique to PPARs, but it may be generally applicable to the protein–ligand interactions of other nuclear receptors in which the ligand specificity is determined by the shape complementarity between the pocket and the ligand.

We thank W. Burkart and M. Moyer for amino acid sequencing and B. Wisely and S. Jordan for involvement in the early phase of the project. We also thank R. Nolte, S. Williams, J. Chrzas, and the Industrial Macromolecular Crystallography Association (IMCA) beamline staff for assistance with data collections at 17-ID of the Advanced Photon Source, which was supported by the Office of Science of the U.S. Department of Energy.

1. Willson, T. M., Brown, P. J., Sternbach, D. D. & Henke, B. R. (2000) *J. Med. Chem.* **43,** 527–550.
2. Kliewer, S. A., Lehmann, J. M. & Willson, T. M. (1999) *Science* **284,** 757–760.
3. Issemann, I. & Green, S. (1990) *Nature (London)* **347,** 645–650.
4. Lehmann, J. M., Moore, L. B., Smith-Oliver, T. A., Wilkison, W. O., Willson, T. M. & Kliewer, S. A. (1995) *J. Biol. Chem.* **270,** 12953–12956.
5. Oliver, W. R., Shenk, J. L., Snaith, M. R., Russell, C. S., Plunket, K. D., Bodkin, N. L., Lewis, M. C., Winegar, D. A., Sznaidman, M. L., Lambert, M. H., *et al.* (2001) *Proc. Natl. Acad. Sci. USA* **98,** 5306–5311. (First Published April 17, 2001; 10.1073/pnas.091021198)
6. Sorbera, L. A., Leeson, P. A., Martin, L. & Castañer, J. (2001) *Drugs Future* **26,** 354–363.
7. Nolte, R. T., Wisely, G. B., Westin, S., Cobb, J. E., Lambert, M. H., Kurokawa, R., Rosenfeld, M. G., Willson, T. M., Glass, C. K. & Milburn, M. V. (1998) *Nature (London)* **395,** 137–143.
8. Uppenberg, J., Svensson, C., Jaki, M., Bertilsson, G., Jendeberg, L. & Berkenstam, A. (1998) *J. Biol. Chem.* **273,** 31108–31112.
9. Gampe, R. T., Jr., Montana, V. G., Lambert, M. H., Miller, A. B., Bledsoe, R. K., Milburn, M. V., Kliewer, S. A., Willson, T. M. & Xu, H. E. (2000) *Mol. Cell* **5,** 545–555.
10. Xu, H. E., Lambert, M. H., Montana, V. G., Parks, D. J., Blanchard, S. G., Brown, P. J., Sternbach, D. D., Lehmann, J. M., Wisely, G. B., Willson, T. M., *et al.* (1999) *Mol. Cell* **3,** 397–403.
11. Henke, B. R., Blanchard, S. G., Brackeen, M. F., Brown, K. K., Cobb, J. E., Collins, J. L., Harrington, W. W., Jr., Hashim, M. A., Hull-Ryde, E. A., Kaldor, I., *et al.* (1998) *J. Med. Chem.* **41,** 5020–5036.
12. Otwinowski, Z., Issacs, N. & Burley, S. (1993) in *Proceedings of the CCP4 Study Weekend*, ed. Sawyer, L. (Science and Engineering Research Council, Daresbury Laboratory, Daresbury, U.K.), pp. 55–62.
13. Collaborative Computational Project Number 4 (1994) *Acta Crystallogr. D* **50,** 760–776.
14. Brunger, A. T., Adams, P. D., Clore, G. M., DeLano, W. L., Gros, P., Grosse-Kunstleve, R. W., Jiang, J. S., Kuszewski, J., Nilges, M., Pannu, N. S., *et al.* (1998) *Acta Crystallogr. D* **54,** 905–921.
15. Lambert, M. H. (1997) in *Practical Application of Computer-Aided Drug Design*, ed. Charifson, P. S. (Dekker, New York), pp. 243–303.
16. Connolly, M. L. (1983) *Science* **221,** 709–713.
17. Nicholls, A., Sharp, K. & Honig, B. (1991) *Proteins* **11,** 281–296.
18. Onate, S. A., Tsai, S. Y., Tsai, M.-J. & O'Malley, B. W. (1995) *Science* **270,** 1354–1357.
19. Kliewer, S. A., Forman, B. M., Blumberg, B., Ong, E. S., Borgmeyer, U., Mangelsdorf, D. J., Umesono, K. & Evans, R. M. (1994) *Proc. Natl. Acad. Sci. USA* **91,** 7355–7359.
20. Takada, I., Yu, R. T., Xu, H. E., Lambert, M. H., Montana, V. G., Kliewer, S. A., Evans, R. M. & Umesono, K. (2000) *Mol. Endocrinol.* **14,** 733–740.
21. Doyle, D. F., Mangelsdorf, D. J. & Corey, D. R. (2000) *Curr. Opin. Chem. Biol.* **4,** 60–63.
22. Murakami, K., Tobe, K., Ide, T., Mochizuki, T., Ohashi, M., Akanuma, Y., Yazaki, Y. & Kadowaki, T. (1998) *Diabetes* **47,** 1841–1847.
23. Goettlicher, M., Widmark, E., Li, Q. & Gustafsson, J. A. (1992) *Proc. Natl. Acad. Sci. USA* **89,** 4653–4657.
24. Goettlicher, M., Demoz, A., Svensson, D., Tollet, P., Berge, R. K. & Gustafsson, J. A. (1993) *Biochem. Pharmacol.* **46,** 2177–2184.
25. Kliewer, S. A., Sundseth, S. S., Jones, S. A., Brown, P. J., Wisely, G. B., Koble, C., Devchand, P., Wahli, W., Willson, T. M., Lenhard, J. M., *et al.* (1997) *Proc. Natl. Acad. Sci. USA* **94,** 4318–4323.
26. van Roermund, C. W. T., Tabak, H. F., van den Berg, M., Wanders, R. J. A. & Hettema, E. H. (2000) *J. Cell Biol.* **150,** 489–497.
27. Barnett, P., Tabak, H. F. & Hettema, E. H. (2000) *Trends Biochem. Sci.* **25,** 227–228.
28. Treisman, J., Gonczy, P., Vashishtha, M., Harris, E. & Desplan, C. (1989) *Cell* **59,** 553–562.
29. Hanes, S. D. & Brent, R. (1989) *Cell* **57,** 1275–1283.
30. Czerny, T. & Busslinger, M. (1995) *Mol. Cell. Biol.* **15,** 2858–2871.
31. Kissinger, C. R., Liu, B. S., Martin-Blanco, E., Kornberg, T. B. & Pabo, C. O. (1990) *Cell* **63,** 579–590.
32. Xu, W., Rould, M. A., Jun, S., Desplan, C. & Pabo, C. O. (1995) *Cell* **80,** 639–650.
33. Xu, H. E., Rould, M. A., Xu, W., Epstein, J. A., Maas, R. L. & Pabo, C. O. (1999) *Genes Dev.* **13,** 1263–1275.